Title

Design of an artificial photosynthetic system for production of alcohols in high concentration from CO 2

Journal

Energy & Environmental Science, 9(1)

ISSN

1754-5692

Authors

Singh, Meenesh R
Bell, Alexis T

Publication Date

2016

DOI

10.1039/c5ee02783g

Peer reviewed

Design of an Artificial Photosynthetic System for Production of Alcohols in High Concentration from CO_2

Meenesh R. Singh[1], and Alexis T. Bell[1,2]*

[1]Joint Center for Artificial Photosynthesis, Material Science Division, Lawrence Berkeley National Laboratory, Berkeley CA 94720

[2]Department of Chemical & Biomolecular Engineering, University of California, Berkeley CA 94720

Corresponding Author:

Professor Alexis T. Bell
The Dow Professor of Sustainable Chemistry
Department of Chemical & Biomolecular Engineering
107 Gilman Hall
University of California
Berkeley, CA 94720-1462
Tel: (510) 642-1536
Email: alexbell@berkeley.edu

Keywords: Artificial Leaf, Renewable Energy, Carbon Dioxide Reduction, Liquid Fuel Separation.

Abstract

Artificial photosynthesis of liquid fuels is a potential source for clean energy. Of particular interest is the formation of alcohols because Alcohols are particularly attractive products because of their high energy density and market value per amount of energy input. The major challenges in photo/electrochemical synthesis of alcohols from sunlight, water and CO_2 are low product selectivity, high membrane fuel crossover losses, and high cost of product separation from the electrolyte. Here we propose an artificial photosynthesis scheme for direct synthesis and separation to almost pure ethanol with minimum product crossover using saturated salt electrolytes. The ethanol produced in the saturated salt electrolytes can be readily phase separated into a microemulsion, which can be collected as pure products in a liquid-liquid extractor. A novel design of an integrated artificial photosynthetic system is proposed that continuously produces >90 wt% pure ethanol using a polycrystalline copper anode and an IrO_2 cathode at a current density of 0.85 mA cm^{-2}. The annual production rate of > 90 wt% ethanol using such a photosynthesis system operating at 10 mA cm^{-2} (12% solar-to-fuel (STF) efficiency) can be 15.27 million gallons per year per square kilometer, which corresponds to 7% of the industrial ethanol production capacity of California.

1. Introduction

An efficient, stable, and scalable artificial photosynthetic system could provide a sustainable source of carbon-neutral fuels. Solar-driven photo-electrochemical CO_2 reduction (CO2R) devices based on various catalysts and light absorbers with varying levels of integration have been demonstrated experimentally,[1-5] and investigated theoretically in detail.[6, 7] Such devices typically operate at near-neutral pH using bicarbonate electrolyte, cation- or anion-exchange membrane, and pure CO_2 feed. The products produced with highest selectivity include H_2, CO, CH_4, C_2H_4, HCOOH, CH_3OH, C_2H_5OH, and C_3H_7OH. The selectivity to these gaseous and liquid products strongly depends on the choice catalyst.[8] It is notable that liquid fuels, such as alcohols, have higher energy density (~20 MJ L^{-1}) and higher market value per amount of energy input (~10 ¢ kW-h^{-1}) than light hydrocarbons, such as methane and ethene.[7]

In contrast to gaseous products, alcohols have much higher solubility in the electrolyte and hence are more difficult to separate.[9] The higher solubility of alcohols also leads to higher membrane-crossover losses due to oxidation of these products at the anode. Another issue is the low concentration of alcohols present in the catholyte. For example, the maximum achievable concentration of ethanol is < 1 mol% when the rate of ethanol generation is equal to 10 mA cm^{-2} and the membrane separating the catholyte from the anolyte is Nafion.[10 11] The energy required to distill such low concentrations of ethanol from the electrolyte is approximately 40.68/0.01= 4068 kJ mol^{-1}, which is much higher than its lower heating value of 1235 kJ mol^{-1}.[7] Alternatively, the catholyte can be heated to evaporate a dilute ethanol-water stream, which can be catalytically upgraded to a C3-C15 blendstock by passage over a zeolite catalysts.[12] However, such upgrading also reduces the net energy efficiency for converting sunlight to fuels. Consequently, there is a need for developing an artificial photosynthetic system that can separate alcohols from the electrolyte directly with minimum membrane crossover losses and energy demand for product concentration.

Separation of alcohols from water is challenging due to formation of azeotropic mixtures. The two widely employed techniques to separate alcohol-water mixtures are distillation and extraction. Distillation of alcohol-water mixtures (< 10 mol%) requires multiple distillation columns and is an energy intensive process.[13] As an alternative, alcohol-water mixtures can be separated into two immiscible, water-rich and alcohol-rich, phases by the addition of salts.[14-17] In this technique, the raffinate phase requires downstream processing to recover salt by evaporating excess water. Alcohol separation using salt has been studied extensively,[15-18] and implemented for the separation of alcohol from dilute aqueous solutions present in fermenters.[14] Based on the same principle, we propose the operation of electrolyzers with saturated salt electrolytes that allows instantaneous phase-separation of alcohols at the cathode into microemulsion, which can be readily collected as pure products without requiring a salt-recovery system. Therefore the objective of this study is to evaluate an artificial photosynthetic system that integrates production and separation of alcohols, focusing on ethanol for illustrative purposes.

2. **Modeling**

2.1 Mass Balance of Liquid Fuels in a Solar-Fuel Generator

A simple mass balance on the alcohol in catholyte can be developed based on the production of alcohol at the cathode and the amount of alcohol diffusing across the membrane separating anolyte and catholyte.

$$V \frac{dc}{dt} = \frac{A_c\, i}{n\, F} - \frac{A_m\, D\, K\, c}{L} \tag{1}$$

where V is the volume of catholyte, c is the molar concentration of alcohol, t is the time, A_c is the area of cathode, i is the partial current density of the alcohol, n is the number of electrons transferred per mole of fuel, F is the Faraday's constant, A_m is the area of membrane separating anolyte and catholyte, D is the diffusion coefficient of alcohol in the membrane, K is the partition coefficient of alcohol between the membrane and the electrolyte, and L is the thickness of the membrane. The permeability of alcohol through the membrane is given as $P = DK/L$. Here we neglect the loss of alcohol due to evaporation, which will decrease the concentration of alcohol as predicted by equation (1). Furthermore, we assume that the concentration of alcohol in the anolyte is negligible, since the kinetic overpotential for its oxidation will be much greater than 1.23 V, which also suggests that the rate of crossover of alcohol through the membrane is much slower than the rate of its oxidation at the anode.

The solution of equation (1) provides the concentration of alcohol as a function of current density and membrane properties, such that

$$c = \frac{A_c\, i}{n\, F\, A_m\, P}\left(1 - e^{-\frac{A_m\, P}{V} t}\right) \tag{2}$$

The steady-state value of c provides the maximum achievable concentration of alcohol when its net production is zero,

$$c_s = \frac{A_c\, i}{n\, F\, A_m\, P} \tag{3}$$

and the time required to reach 99% of steady-state concentration is given by

$$t_s = -\frac{\ln(0.01)\, V}{A_m\, P} \tag{4}$$

The time required to reach maximum concentration does not depend on the operating current density and is only a function of membrane properties and volume of catholyte.

2.2 Phase Equilibrium of Salt-Ethanol-Water Mixtures

The solubility of organic molecules in aqueous systems decreases with increase in the salt concentration, and the phase equilibrium for salt-water-organics mixtures have been thoroughly investigated for various systems.[15] Phase separation of alcohols in saturated salt electrolytes is due to the "salting-out" effect, a phenomenon in which salt binds strongly with water thereby weakening the water organic interactions and causing the organic to phase separate.[19] The phase diagram of salt-organics-water mixtures has a binodal curve dividing the two-phase from the single, miscible phase region and tie lines representing the equilibrium composition of the liquid phases, which are strongly dependent of the salt composition and temperature. While various salts might be used as electrolytes, cesium carbonate is particularly attractive because is known to promote CO_2 reduction,[20-22] and can also be used to phase-separate ethanol produced at the cathode.[16] The experimentally measured binodal curve for cesium carbonate-water-ethanol mixture at 20℃ is given by the following empirical equation[16]:

$$\ln w_1 = -0.064 - 1.477\, w_2^{0.5} - 1.481\, w_2 - 2.749\, w_2^{2} - 2.872\, w_2^{3} \tag{5}$$

where w_1 and w_2 are the weight fractions of ethanol and cesium carbonate, respectively. The tie lines have also been measure experimentally [16] and are described by

$$\frac{1-w_1^E}{w_1^E} = 0.74\left(\frac{1-w_2^R}{w_2^R}\right)^{1.769} \tag{6}$$

where w_1^E is the weight fraction of ethanol in the extract (top) phase, and w_2^R is the weight fraction of cesium carbonate in the raffinate (bottom) phase.

3. Results and Discussion

3.1 Achievable Concentrations of Liquid Fuels

Figure 1a shows the increase in the steady-state concentrations of formic acid, methanol, ethanol, and propanol as functions of the cell current densities. These concentrations were determined assuming equal areas of catalyst (same as the area of the cathode) and ion-exchange membrane, and are based on the permeability of formic acid,[23] and alcohols[11] through Nafion 117. The steady-state concentration of formic acid is higher than that of alcohols because of its higher stoichiometric number (0.5) per electron transferred. Since the diffusion coefficient of alcohols in Nafion 117 decreases with increasing the size of the alcohol, the steady-state concentration of alcohol increases with increasing alcohol size. It should be noted, though, that high product concentration can only be achieved at high (> 100 mA/cm^2) product current densities and require very long (> 45 h) times to reach 99% of the steady-state concentration.

Artificial photosynthetic systems are usually limited by light absorption and therefore operate at product current densities < 10 mA cm^{-2}.[7] Reference to Fig. 1a shows that achievable concentrations at this current density are 4.4 mol% for formic acid, 0.4 mol% for methanol, 0.6 mol% for ethanol, and 1.2 mol% for propanol. These concentrations can be increased by using an ion-exchange membrane with lower fuel permeabilities than Nafion 117. Figure 1b shows the steady-state concentrations of liquid fuels at 10 mA cm^{-2} increases with decreasing membrane permeability $\left(DK/L\right)$. It can be seen that an order of magnitude decrease in the membrane mass-transfer coefficient increases the concentration of formic acid up to 32 mol%, methanol up to 4 mol%, ethanol up to 5 mol%, and propanol up to 11 mol%. This analysis provides an upper limit on the achievable concentrations of liquid fuel in the artificial photosynthetic system using a state-of-the-art ion-exchange membrane with an order of magnitude lower fuel permeability than characteristic of Nafion 117.

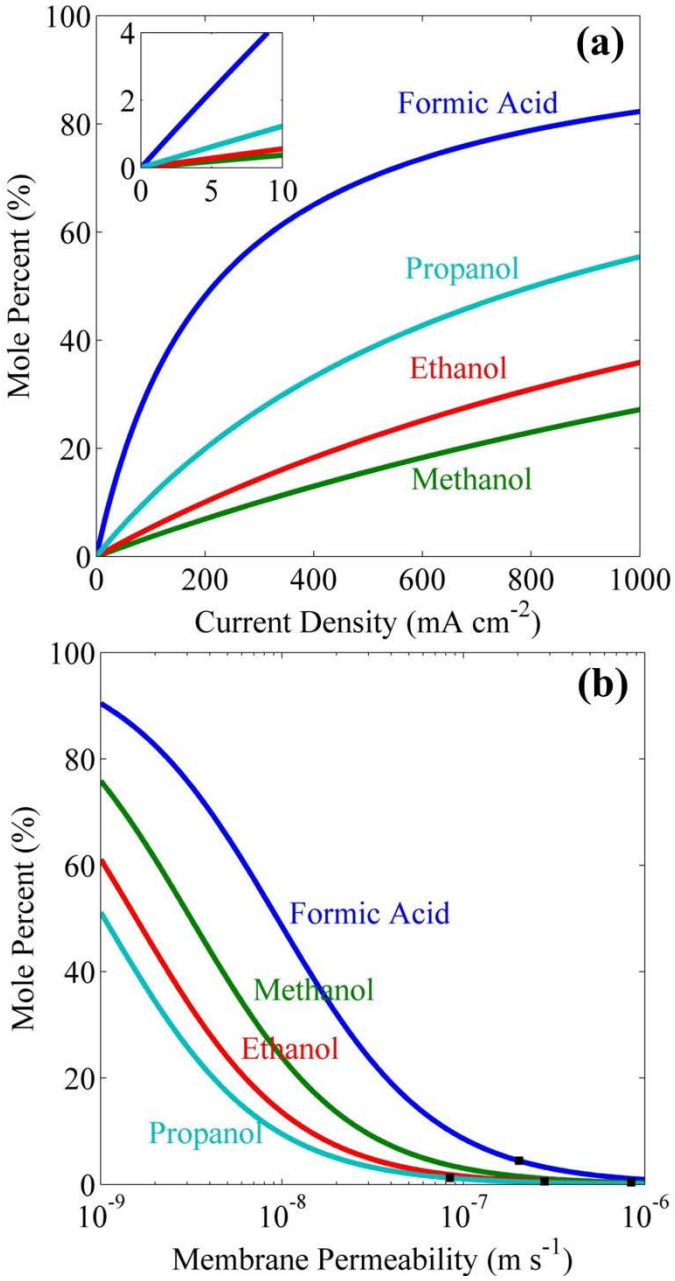

Figure 1: a) Maximum concentration of formate, methanol, ethanol, and propanol versus current density, b) Maximum concentration of formate, methanol, ethanol, and propanol versus membrane permeability. The permeabilities of these products through Nafion 117 are shown by black squares.

3.2 Phase Diagram of Cesium Carbonate-Water-Ethanol Mixtures

Figure 2 shows the binodal curve (or solubility curve) for ethanol and cesium carbonate in water, obtained using equation (5). Ethanol and water are completely miscible; however, slight addition of cesium carbonate drastically reduces the solubility of ethanol to 60 mol%. The

solubility of ethanol can be further decreased by increasing the concentration of cesium carbonate. The lowest concentration of ethanol is 0.9 mol% at the solubility limit of cesium carbonate in water (13 mol%). On the left side of the binodal curve, all three components of the mixture coexist in one liquid phase. On the right side of the binodal curve, an ethanol-rich microemulsion can be formed in the water-rich phase. The composition of the emulsion is given by the tie lines (dotted lines) in Figure 2, which are obtained using equation (6). The left end of the tie line is the composition of the extract phase (the ethanol-rich phase) and the right end of the tie line is the composition of the raffinate phase (the water-rich phase). There is an interesting region in the phase diagram of cesium carbonate-water-ethanol mixtures, where three phases such as ethanol-rich, water-rich, and hydrates of cesium carbonate can coexists. The concentration of ethanol in the extract phase of this triple-phase region can be as high as 100 mol%.

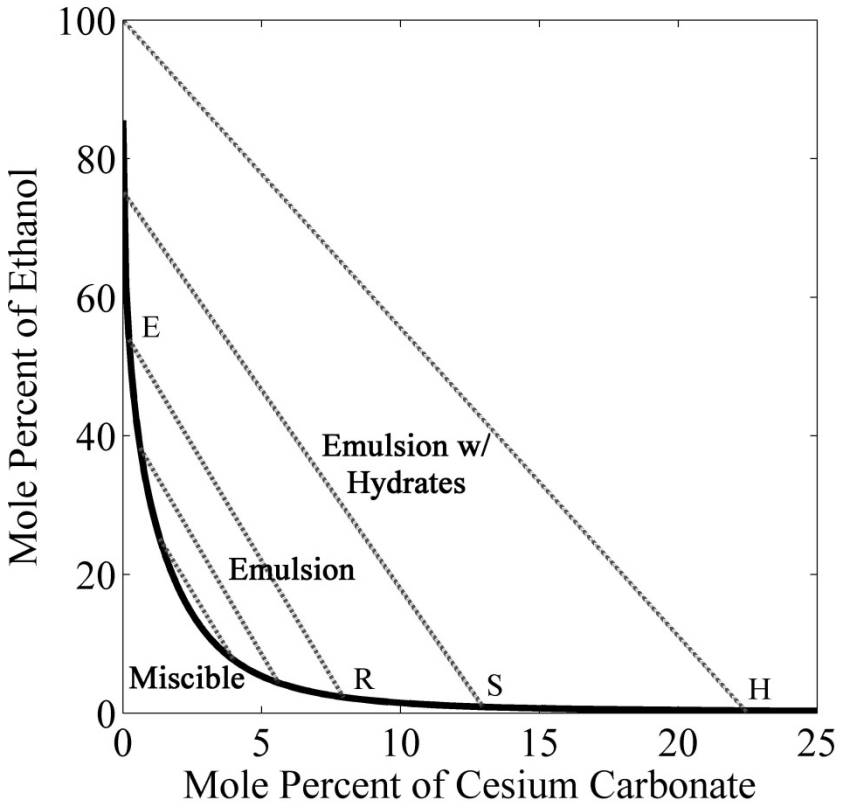

Figure 2: Liquid-liquid phase equilibrium showing binodal curve and tie lines for a mixture of ethanol, water, and cesium carbonate measured at 20℃. E and R are the composition of the extract and raffinate phases joined by the tie line. S is the solubility limit of cesium carbonate in water. H is the state of cesium carbonate hydrate formation corresponding to 100% ethanol in the extract phase.

3.4 Advanced Artificial Photosynthetic System

Figure 3 shows a scheme for a photosynthetic system utilizing salt-based, liquid-liquid extraction of fuels. In this scheme, a photoelectrochemical cell or PV-electrolyzer can be used consisting of photoanode or anode, a porous cathode with a gas-diffusion layer impregnated with a saturated salt (Cs_2CO_3) electrolyte. The anolyte compartment is separated from the catholyte compartment by an anion-exchange membrane (AEM). Since CO_2 is sparingly soluble in a saturated salt electrolyte,[24] it must be supplied through a gas-diffusion layer. Electrochemical reduction of gaseous CO_2 in such cell configuration has been tested at current densities > 300 mA cm^{-2}.[25, 26] A continuous flow of catholyte is required to collect CO_2 reduction products, so that they do not contaminate the CO_2 feed. Based on the phase equilibrium thermodynamics for the cesium carbonate-water-ethanol system shown in Figure 2, the ethanol produced at the cathode will form a microemulsion in the saturated cesium carbonate electrolyte. The microemulsion is then fed to a settler, where it passes through a coalescer and is collected as a liquid containing > 90 wt% pure ethanol. The make-up water feed to the settler balances the amount of water removed with the extract phase and consumed at the cathode. The bottom phase containing salt and water is recycled to the photo/electrochemical cell.

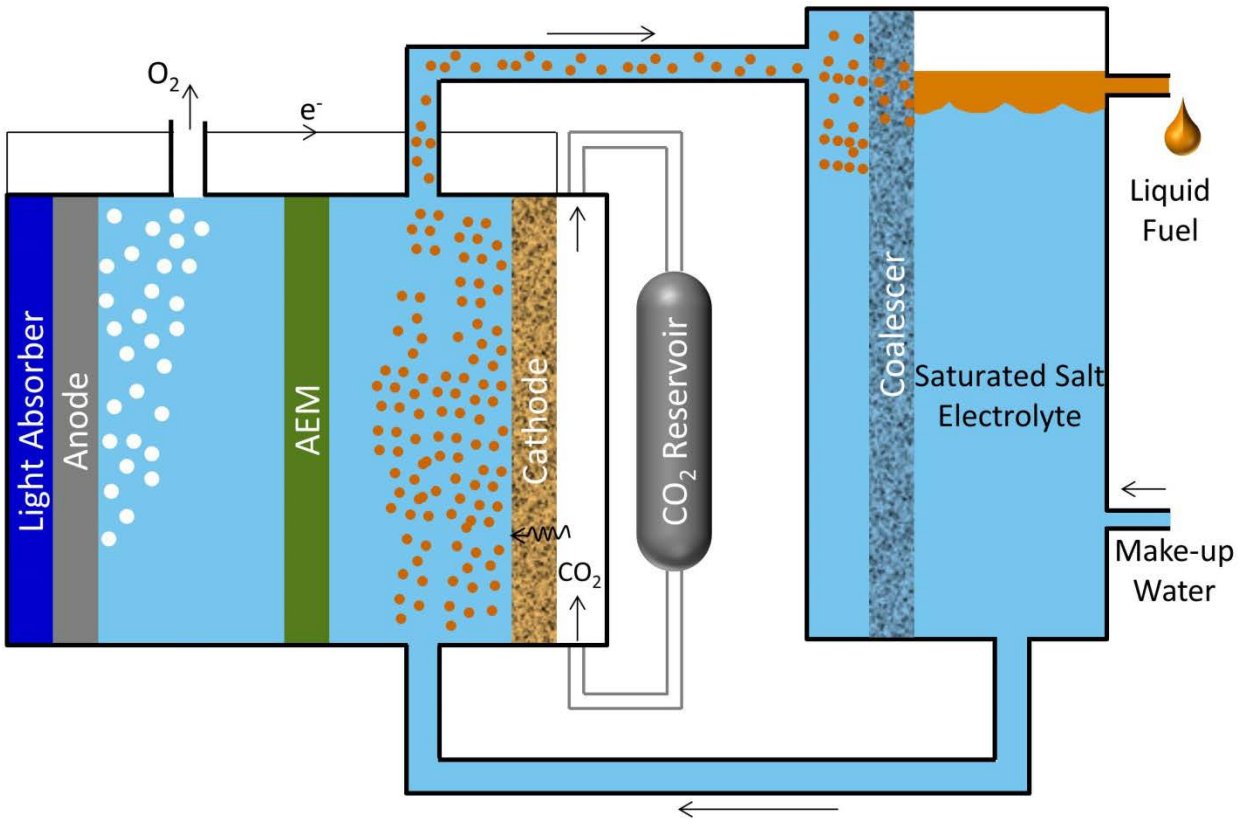

Figure 3: Schematic of advanced artificial photosynthetic system connecting a photoelectrochemical cell or PV-Electrolyzer with a liquid-liquid extractor. The liquid fuels are

directly converted into microemulsion at the cathode surface in presence of saturated salt electrolyte. The microemulsion is separated into concentrated liquid fuels using a settler.

Figure 4 shows the equilibrium concentration of ethanol in the extract and the raffinate phases as a function of the concentration of cesium carbonate. The concentration of ethanol reaches 75.7 mol% (or 92.9 wt%) in the extract phase and 0.87 mol% (or 0.6 wt%) in the raffinate phase, when the Cs_2CO_3 reaches its solubility limit (13 mol%) in water. Ethanol in the raffinate phase will diffuse across the anion-exchange membrane and undergo oxidization at the anode. The crossover current density of ethanol is given as

$$i_{crossover} = n\,F\,P\,c \tag{7}$$

Figure 4 also shows that as the ethanol concentration decreases with increasing salt concentration, the crossover current density of ethanol through Nafion 117 also decreases due to the lower concentration of ethanol in the raffinate. At saturation limit of Cs_2CO_3 in water, the crossover current density corresponding to the ethanol concentration of 0.87 mol% in raffinate phase is 10.6 mA cm^{-2}. What this means is that to produce an ethanol-rich microemulsion, the partial current density of ethanol must be greater than the expected crossover current density of 10.6 mA cm^{-2}. This constraint is challenging because reported partial current densities of ethanol are only of the order of 1 mA cm^{-2}.[27]

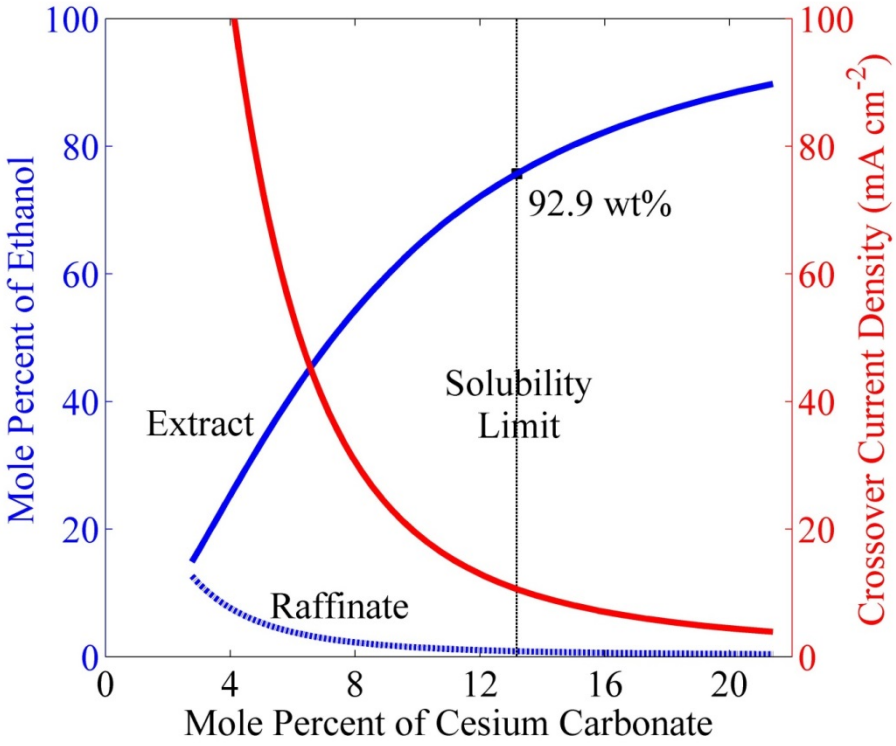

Figure 4: Equilibrium concentration of ethanol in the extract and the raffinate streams versus concentration of cesium carbonate. The crossover current density decreases with decreasing concentration of ethanol in the raffinate.

Polycrystalline copper can produce 0.85 mA cm^{-2} of ethanol with a Faradaic efficiency (FE) of 11% at about -1.1 V vs RHE.[10, 27] A photo/electrochemical cell consisting of IrO_2 anode and Cu cathode separated by Nafion 117 can be operated at -1.1 vs RHE to generate such current densities in Cs_2CO_3 electrolyte.[20] However, as noted above, rate of ethanol generation is well below the threshold current density to form a microemulsion in a 13 wt% $CsCO_3$ solution (10.6 mA/cm^2), and all of the ethanol produced will cross over to the anolyte compartment and be consumed. One way to circumvent this situation is to increase the ratio of catalyst-to-membrane areas well above 1.0. Figure 5a shows the increase in catholyte ethanol concentration with increasing ratio of Cu catalyst area to Nafion 117 area for two different electrolytes - 1 mol% and 13 mol% cesium carbonate and an ethanol partial current density of 0.85 mA cm^{-2}. It can be seen that the ethanol concentration in 1 mol% Cs_2CO_3 only be increased to 4.5 mol% by increasing the catalyst-to-membrane area ratio to 100. Reference to Figure 2 shows that ethanol will not phase-separate in 1 mol% Cs_2CO_3 because the required concentration of ethanol for phase-separation is 30 mol%. However, the required ethanol concentration for phase-separation is only 0.87 mol% in 13 mol% Cs_2CO_3, a level can be attained by increasing the catalyst-to-membrane area ratio to > 18.46. Under these circumstances, the microemulsion will contain 93 wt% ethanol. Although the formation of microemulsion is only dependent on the partial current density of ethanol and the catalyst-to-membrane area, the FE of ethanol formation can affect the current and voltage efficiencies which directly affect the solar-to-fuel (STF) efficiency of this process. Increasing the FE of ethanol to >11% will decrease the side-reactions (which will increase the current efficiency) and also reduce the ohmic losses associated with the side-reactions (which will increase the voltage efficiency). Therefore, identification of novel catalysts that can produce ethanol at higher FE (>11%) and current density (> 1 mA cm^{-2}) will not only increase the productivity ethanol microemulsion but will also increase its efficiency.

There are two consequences of increasing the catalyst-to-membrane areas. The first is a decrease in the ethanol-crossover current density and the second is an increase in the ohmic loss across the membrane. Figure 5b shows that the crossover current density is equal to the ethanol current density until the onset of phase separation occurs at the catalyst-to-membrane (Cu cathode-to-Nafion membrane) area ratio of 18.46, after which the crossover current density rapidly decreases with further increasing catalyst-to-membrane area ratio, since the ethanol in the electrolyte is already at the saturation limit. The ohmic loss across the membrane increases linearly with increasing catalyst-to-membrane area ratio, and for the area ratio of 18.46 the crossover current density is equal to 0.6 mA/cm^2, which means that the net rate of ethanol formation will be 0.85 – 0.60 = 0.25 mA cm^{-2}; however, the ohmic loss across the membrane will only be 20 mV. The crossover current density could be reduced from 0.6 mA cm^{-2} to 0.1 mA

cm^{-2} by decreasing the membrane ethanol permeability by six fold relative to Nafion 117, and in this case, the net ethanol current density will become 0.85 - 0.1 = 0.75 mA cm^{-2}.

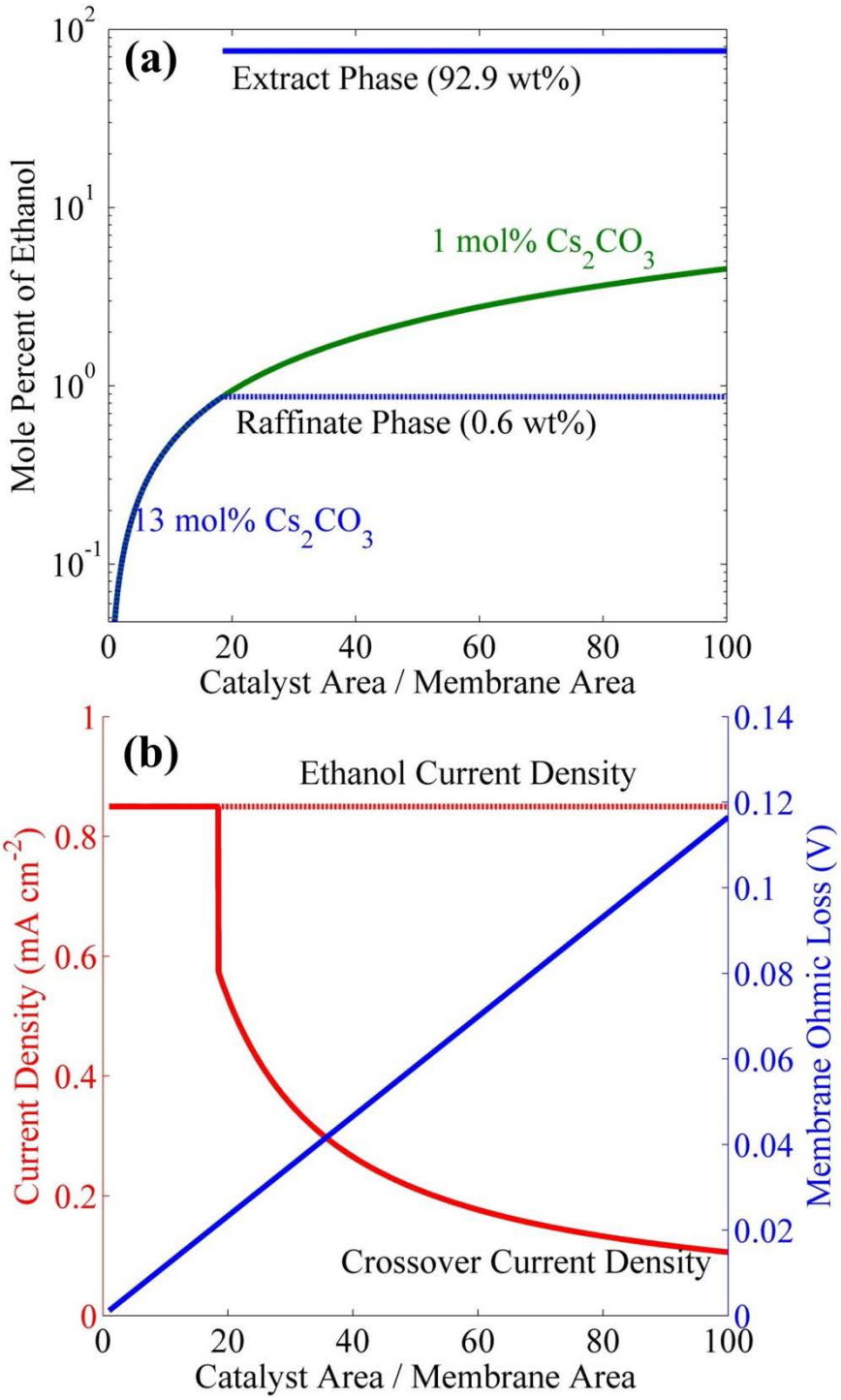

Figure 5: a) Steady-state concentration of ethanol in 1 mol% (dilute) and 13 mol% (saturated) cesium carbonate electrolyte versus ratio of catalyst-to–membrane (Cu cathode-to-Nafion membrane) area, at 0.85 mA cm^{-2} partial current density of ethanol. b) Membrane ohmic loss and

crossover current density of ethanol in dilute and saturated electrolytes versus ratio of catalyst-to-membrane area.

Under such conditions, increasing the partial current density of ethanol will not change its concentration in the microemulsion but will increase the volumetric flowrate of emulsion. The net molar flow rate of ethanol can be written as

$$\frac{A_c\left(i - i_{crossover}\right)}{n\,F} = c_1^E\,q\,, \tag{8}$$

where c_1^E is the molar concentration of ethanol in the extract phase, and q is the flowrate of the extract phase. Figure 6 shows that the flowrate of extract phase containing 93 wt% ethanol increases linearly with increasing partial current density above the crossover current density of 0.1 mA cm^{-2}. The corresponding increase in the STF efficiency will be 1.2% to 12% for the increase in the partial current density from 1 mA cm^{-2} to 10 mA cm^{-2}. The flowrate of the 93 wt% ethanol phase is ~5.5 L s^{-1} when produced over a square kilometer area at an ethanol partial current density of 10 mA cm^{-2}. The annual production rate of ethanol assuming 8h of active operation per day at 10 mA cm^{-2} (or 12% STF efficiency) is 15.27 million gallons per year, which is 7% of the current fuel ethanol production rate of 218 million gallons per year in California.[28] This analysis shows the viability of the proposed scheme for producing ethanol at a rate comparable to that of a typical ethanol plant[28] in California.

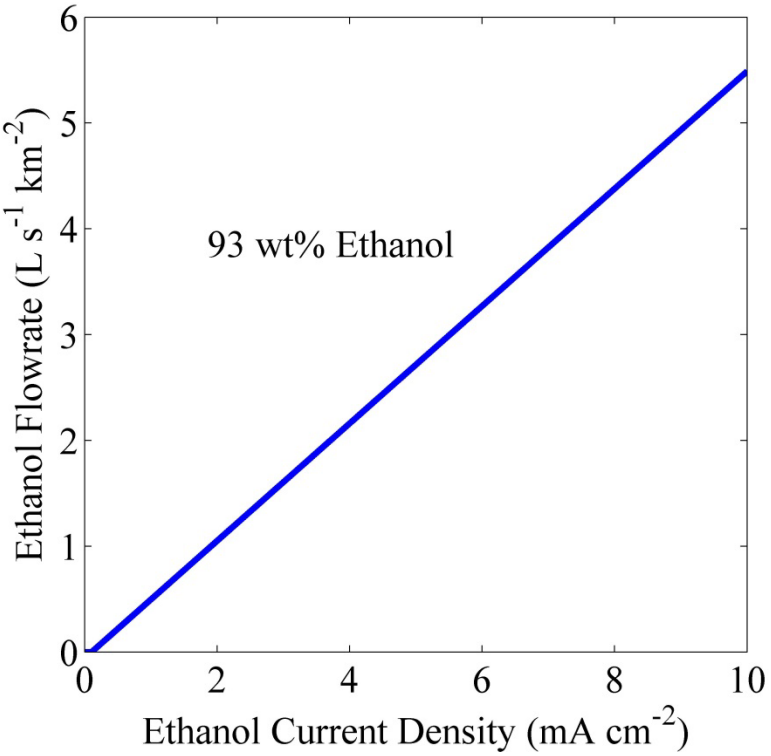

Figure 6: Flowrate of 93 wt% ethanol generated over a square kilometer area versus partial current density. Electrolyte is 13 mol% Cs_2CO_3 and the crossover current density is 0.1 mA cm^{-2}.

Although the proposed scheme should be able to produce pure liquid products continuously, there can be some operational challenges. These include i) stability of materials used to make the cell in saturated Cs_2CO_3 electrolyte of pH = 10, ii) power required to pump saturated Cs_2CO_3 electrolyte, and iii) crystallization of salt due to electrodialysis. We consider that these concerns are all surmountable for the following reasons. Advances in electrolysis alkaline electrolytes have led to the development of various materials that are stable in base.[29] For example, acrylic polymer can be used for the cell body, Selemion for the membrane, copper for the cathode, and IrO_2 for anode, all of which are known to be stable in an alkaline environment. The viscosity of saturated CsCl electrolyte is 0.87 cP;[30] therefore, if we assume a similar viscosity for Cs_2CO_3, the pumping requirement will be similar to that for water. Setting a suitably high flowrate of catholyte would not only increase the collection efficiency of the microemulsion but also decrease the supersaturation of salt and its crystallization at the cathode.

4. Conclusions

We have summarized the challenges associated with the production of pure alcohol fuels such methanol, ethanol, and propanol using artificial photosynthesis and provide a scheme to benefit such production. The maximum achievable concentrations of various alcohols in the catholyte are of the order of 1 mol % at partial current densities of 10 mA cm^{-2}. However such concentrations can only be achieved about 100 h of batch operation and result in in 100% fuel-crossover if a Nafion 117 membrane is used to separate the catholyte and anolyte compartments. Reducing the alcohol permeability of the ion-exchange membrane by an order of magnitude only increases the liquid fuel concentration to 10 mol%, but also raises the batch operation time needed to achieve this concentration to 1000 h. To overcome these limitations, we propose an artificial photosynthetic system (Figure 3) that utilizes concentrated salt electrolytes to phase-separate ethanol (or other organics) into microemulsion; and thereby reduce alcohol crossover and increase product collection efficiency. The proposed system has an additional advantage; it does not require a salt-recovery process and the phase-separated salt-water mixture can be re-circulated back to the photo/electrochemical cell. The use of cesium carbonate as the electrolyte and a gas-diffusion electrode will enhance the rate of CO_2 reduction reaction.[20, 25, 26] We show that photo/electrochemical reduction using 13 mol% cesium carbonate, and a catalyst-to-membrane area of 100 (or a catalyst-to-membrane area of 18.46 with a membrane ethanol permeability six-fold lower than that of Nafion 117) results in the formation of a microemulsion containing 93 wt% ethanol, while still producing 0.85 mA cm^{-2} ethanol at 0.1 mA cm^{-2} of crossover and an ohmic loss across the membrane of 117 (or 20) mV. The annual production rate of 93 wt% ethanol produced directly from such artificial photosynthetic system operating at 10

mA cm^{-2} (or 12% STF efficiency) will be 15.27 million gallons per year per square kilometer, which is 7% of the capacity for industrial ethanol production in California.

5. Acknowledgements

This material is based on the work performed by the Joint Center for Artificial Photosynthesis, a DOE Energy Innovation Hub, supported through the Office of Science of the U.S. Department of Energy under Award number DE-SC0004993.

References

1. T. Sekimoto, S. Shinagawa, Y. Uetake, K. Noda, M. Deguchi, S. Yotsuhashi and K. Ohkawa, *Applied Physics Letters*, 2015, **106**, 073902.
2. Y. Sugano, A. Ono, R. Kitagawa, J. Tamura, M. Yamagiwa, Y. Kudo, E. Tsutsumi and S. Mikoshiba, *RSC Advances*, 2015, **5**, 54246-54252.
3. J. L. White, J. T. Herb, J. J. Kaczur, P. W. Majsztrik and A. B. Bocarsly, *Journal of CO2 Utilization*, 2014, **7**, 1-5.
4. T. Arai, S. Sato and T. Morikawa, *Energy & Environmental Science*, 2015, **8**, 1998-2002.
5. M. Schreier, L. Curvat, F. Giordano, L. Steier, A. Abate, S. M. Zakeeruddin, J. Luo, M. T. Mayer and M. Grätzel, *Nature communications*, 2015, **6**.
6. M. R. Singh, E. L. Clark and A. T. Bell, *Physical Chemistry Chemical Physics*, 2015, **17**, 18924-18936.
7. M. R. Singh, E. L. Clark and A. T. Bell, *Submitted to PNAS*, 2015.
8. Y. Hori, in *Modern aspects of electrochemistry*, Springer, 2008, pp. 89-189.
9. D. W. Green, *Perry's chemical engineers' handbook*, McGraw-hill New York, 2008.
10. E. L. Clark, M. R. Singh, Y. Kwon and A. T. Bell, *Analytical Chemistry*, 2015, **87**, 8013-8020.
11. D. Rivin, C. Kendrick, P. Gibson and N. Schneider, *Polymer*, 2001, **42**, 623-635.
12. C. K. Narula and B. H. Davison, Google Patents, 2014.
13. H.-J. Huang, S. Ramaswamy, U. Tschirner and B. Ramarao, *Separation and Purification Technology*, 2008, **62**, 1-21.
14. J. C. Card and L. M. Farrell, *Separation of alcohol-water mixtures using salts*, Oak Ridge National Lab., TN (USA), 1982.
15. H. Zerres and J. Prausnitz, *AIChE journal*, 1994, **40**, 676-691.
16. M. Hu, Q. Zhai and Z. Liu, *Journal of Chemical & Engineering Data*, 2004, **49**, 717-719.
17. M. C. Iliuta, K. Thomsen and P. Rasmussen, *Chemical Engineering Science*, 2000, **55**, 2673-2686.
18. M. Hu, Q. Zhai, Z. Liu and S. Xia, *Journal of Chemical & Engineering Data*, 2003, **48**, 1561-1564.
19. J. M. Prausnitz, R. N. Lichtenthaler and E. G. de Azevedo, *Molecular thermodynamics of fluid-phase equilibria*, Pearson Education, 1998.
20. A. Murata and Y. Hori, *Bulletin of the Chemical Society of Japan*, 1991, **64**, 123-127.
21. G. Kyriacou and A. Anagnostopoulos, *Journal of applied electrochemistry*, 1993, **23**, 483-486.

22. M. R. Thorson, K. I. Siil and P. J. Kenis, *Journal of the Electrochemical Society*, 2013, **160**, F69-F74.
23. Y.-W. Rhee, S. Y. Ha and R. I. Masel, *Journal of Power Sources*, 2003, **117**, 35-38.
24. U. Riebesell, V. J. Fabry, L. Hansson and J.-P. Gattuso, *Guide to best practices for ocean acidification research and data reporting*, Publications Office of the European Union Luxembourg, 2010.
25. R. L. Cook, R. C. MacDuff and A. F. Sammells, *Journal of The Electrochemical Society*, 1990, **137**, 607-608.
26. M. Schwartz, R. L. Cook, V. M. Kehoe, R. C. MacDuff, J. Patel and A. F. Sammells, *Journal of the Electrochemical Society*, 1993, **140**, 614-618.
27. K. P. Kuhl, E. R. Cave, D. N. Abram and T. F. Jaramillo, *Energy & Environmental Science*, 2012, **5**, 7050-7059.
28. http://www.neo.ne.gov/statshtml/122.htm.
29. K. Zeng and D. Zhang, *Progress in Energy and Combustion Science*, 2010, **36**, 307-326.
30. D. E. Goldsack and R. Franchetto, *Canadian Journal of Chemistry*, 1977, **55**, 1062-1072.